

# Experimental Demonstration of Localized Plasmonic Structured Illumination Microscopy

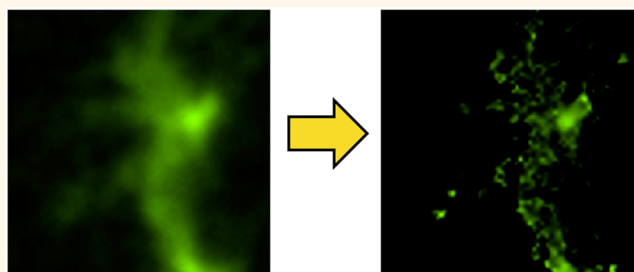
Joseph L. Ponsetto,<sup>†</sup> Anna Bezryadina,<sup>†</sup> Feifei Wei,<sup>‡</sup> Keisuke Onishi,<sup>§</sup> Hao Shen,<sup>†</sup> Eric Huang,<sup>‡</sup> Lorenzo Ferrari,<sup>||</sup> Qian Ma,<sup>†</sup> Yimin Zou,<sup>§</sup> and Zhaowei Liu<sup>\*,†</sup>

<sup>†</sup>Department of Electrical and Computer Engineering, <sup>‡</sup>Department of Physics, <sup>§</sup>Neurobiology Section, Biological Sciences Division, and <sup>||</sup>Materials Science and Engineering, University of California, San Diego, 9500 Gilman Drive, La Jolla, California 92093, United States

## Supporting Information

**ABSTRACT:** Super-resolution imaging methods such as structured illumination microscopy and others have offered various compromises between resolution, imaging speed, and biocompatibility. Here we experimentally demonstrate a physical mechanism for super-resolution that offers advantages over existing technologies. Using finely structured, resonant, and controllable near-field excitation from localized surface plasmons in a planar nanoantenna array, we achieve wide-field surface imaging with resolution down to 75 nm while maintaining reasonable speed and compatibility with biological specimens.

**KEYWORDS:** super-resolution, plasmonics, structured illumination microscopy, fluorescence imaging, nanofabrication



Since Ernst Abbe described the diffraction limit over a century ago, high-resolution optical imaging has become better and better over the years and is now pushing up against theoretical limits. For many active areas of biological research,<sup>1–5</sup> this limit has become a barrier to improved biological understanding. In recent years, surface imaging of various biological dynamics and biomechanical phenomena has seen a surge of interest. Imaging of processes such as exocytosis and kinesin motion are most effective when depth is limited to a very thin region of interest at the edge of the cell or specimen. However, many objects and processes of interest are of size scales far below the diffraction limit for visible light. Many creative methods to circumvent this limitation have been developed, such as structured illumination microscopy (SIM),<sup>6,7</sup> stochastic optical reconstruction microscopy (STORM),<sup>8</sup> the hyperlens,<sup>9,10</sup> stimulated emission depletion (STED),<sup>11</sup> photoactivated localization microscopy (PALM),<sup>12</sup> and the far-field superlens (FSL).<sup>13</sup>

All of these methods have trade-offs between several factors such as resolution, speed, field of view, biocompatibility, sensitivity, and experimental complexity. Localization-based techniques such as STORM and PALM are typically slow, albeit with very high resolution. Other techniques such as STED and saturated SIM (SSIM)<sup>14</sup> require strong intensities, which can harm sensitive biological samples. Standard SIM has seen widespread adoption<sup>15</sup> due to its combination of super-resolution, practicality, and reasonable imaging speed.<sup>16,17</sup> However, since the illumination structure in SIM is itself diffraction-limited, the resolution can be improved only about

2-fold *versus* standard microscopy. Traditional SIM utilizing the best available optics is not enough to bring the resolution down to deep sub-100 nm scales,<sup>18</sup> despite tremendous demand for such a tool in various applications.

It is always possible to improve resolution by decreasing the illumination wavelength. However, this is accompanied by an increase in photon energy, which becomes prohibitive for biosamples even at ultraviolet frequencies. One approach with demonstrated success, plasmonic SIM (PSIM),<sup>19,20</sup> achieves shorter wavelength without increasing the photon energy by taking advantage of surface plasmon polariton (SPP)<sup>21</sup> dispersion at a metal–dielectric interface. The PSIM method has potential for higher resolution, if the dispersion properties can be specially designed and combined with traditional SIM.<sup>22</sup>

## PRINCIPLES OF LPSIM

Taking the push for subwavelength imaging significantly further is a technique, localized plasmonic SIM (LPSIM), demonstrated here in experiment. This technique differs from traditional SIM in a way that allows for a dramatic improvement in performance. The physical behavior relied on for forming our structured illumination patterns is the tight confinement of localized plasmonics fields, rather than propagating wave interference in the case of PSIM. Different

Received: February 18, 2017

Accepted: May 1, 2017

Published: May 3, 2017

from the energy-wavelength relation dictated by either photonic or SPP dispersion, we design a substrate that gives us controlled, tunable, ultrafine illumination patterns, untethered to any dispersion relation. This is accomplished using the localized plasmons (LPs) generated by a carefully designed nanoantenna array.<sup>23</sup> Localized plasmons are bound to the local geometry of a metal–dielectric interface<sup>24</sup> and thus do not have a wavelength, strictly speaking. The spatial frequency of an array of LPs is therefore determined primarily by the local geometry itself, which can be designed arbitrarily and can be much larger than that of light or SPPs, as shown in Figure 1a.

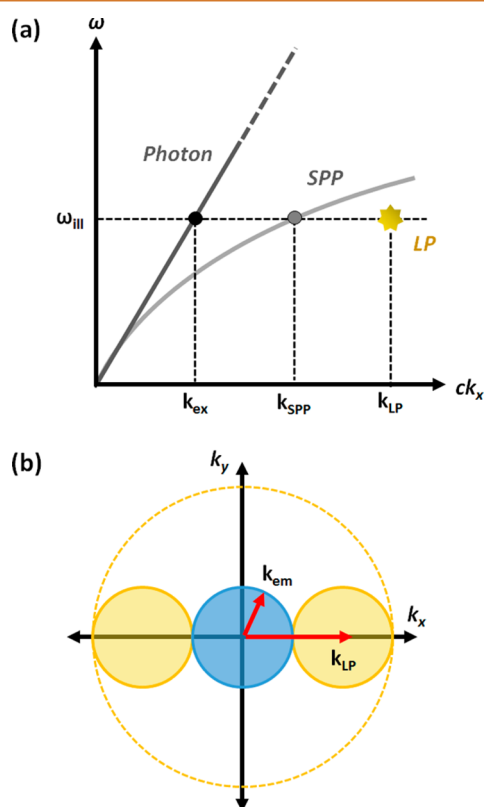


**Figure 1.** (a) Illustrative plot of temporal frequency *versus* wavenumber for the illuminating laser, the PSIM method (light gray curve), and the LP field (gold star) in an example LPSIM experiment. Here,  $k_{LP}$  is the spatial frequency generated by the nanoantenna array, which can be tuned as desired, within fabrication capabilities. (b) Spatial frequency scheme: The collected wavevectors in a traditional image are limited by the emission wavenumber  $k_{em}$  (blue circle). With structured illumination *via* LP fields, this imaging resolution is enhanced dramatically in a controllable manner (gold dashed circle, in this specific example).

The spatial frequency  $k$  of a pattern generated with LPs can thus be dramatically higher than the wavenumber of the fluorescent light which is collected to form the image. Access to higher spatial frequencies in our illumination gives us the ability to achieve higher imaging resolution than previous SIM-based methods. Typical images formed in the far field will have diffraction-limited resolution, as represented by the blue circle in Figure 1b. Under structured illumination, the moiré effect<sup>25</sup> transfers information from higher spatial frequencies into the observable regime of the diffraction-limited optical transfer function (OTF). Fine details from an illuminated object that would normally be impossible to capture with any far-field

optical setup can thus be captured. With knowledge of the illumination structure and the point spread function (PSF) of the imaging system, this high- $k$  information can be shifted back to its origin in Fourier space,<sup>26</sup> enabling super-resolution image reconstruction. This concept is used in all SIM-based techniques, but the degree of resolution improvement is directly tied to the spatial frequencies that the illumination can provide. LPSIM is differentiated in this respect by the very fine structure enabled and dictated by a nanoantenna array through  $k_{LP}$ , which breaks the diffraction limit for propagating waves and allows for the collection of extremely high spatial frequency information. This principle can be applied at different size and wavelength scales, depending on the application. A combination of SIM, PSIM, and LPSIM could be used to fill in a very large effective OTF and provide a 5× or more improvement in resolution over standard optics. However, the  $k_{LP}$  chosen in this proof-of-concept experiment was designed to yield a 3× resolution improvement over a diffraction-limited image, solely by LPSIM (see Figure 1b).

### PLASMONIC NANOANTENNA DESIGN

To generate changeable structured excitation patterns with LP fields, a 2D hexagonal array of silver nanodiscs was illuminated with a laser near the disc dipole resonance. The resulting plasmonic field patterns can be shifted in a controllable manner within the object plane by changing the incident angle and polarization of the laser. These fields excite fluorescent emission in a fluorescent-tagged object (Figure 2, inset).

Figure 2 shows the schematics of the experimental LPSIM setup. The incident angle is controlled by a 2D scanning mirror system in combination with a high numerical aperture (NA) 4f system. The achievable incident angle range in the setup was  $\pm 56^\circ$  in any incident plane. A cylindrical lens was used to account for the spatial offset of the first scanning mirror relative to the 4f system. Fluorescent emission was collected by a 1.2 NA 60× water immersion objective, filtered, and passed through a tube lens for additional magnification. The images were recorded with an electron-multiplying charge-coupled device (EMCCD). Several lasers at various visible frequencies were aligned in parallel at the beginning of the optical path, to allow for easy switching based on the fluorescent dyes present in different objects.

Since the LP fields are determined by local geometry, care was taken in the design and fabrication of our nanoantenna array. The design shown in this work, illustrated in Figure 3a, is just one of many potential LPSIM geometries that can be used to achieve super-resolution of varying degrees. In addition to the geometric parameters, the material properties at the operating frequency are also important. The overall design depends on several criteria that must be met for an effective LPSIM substrate. First, the operating wavelength was chosen to be in the visible range for our imaging application. From there, silver was chosen for its strong plasmonic response at short visible wavelengths.

The geometrical parameters of the structures were chosen such that patterns appropriate for LPSIM could be reliably generated. Three axes of symmetry provided by the hexagonal array scheme give the ability to nearly cover the full  $k$ -space region inside the dashed circle in Figure 1b. This is an improvement over the square design used in PSIM, which gives just two symmetry axes. The pitch of the array is chosen such that the primary spatial frequency  $k_{LP}$  of the excitation pattern will be twice the radius of the diffraction-limited OTF. This is

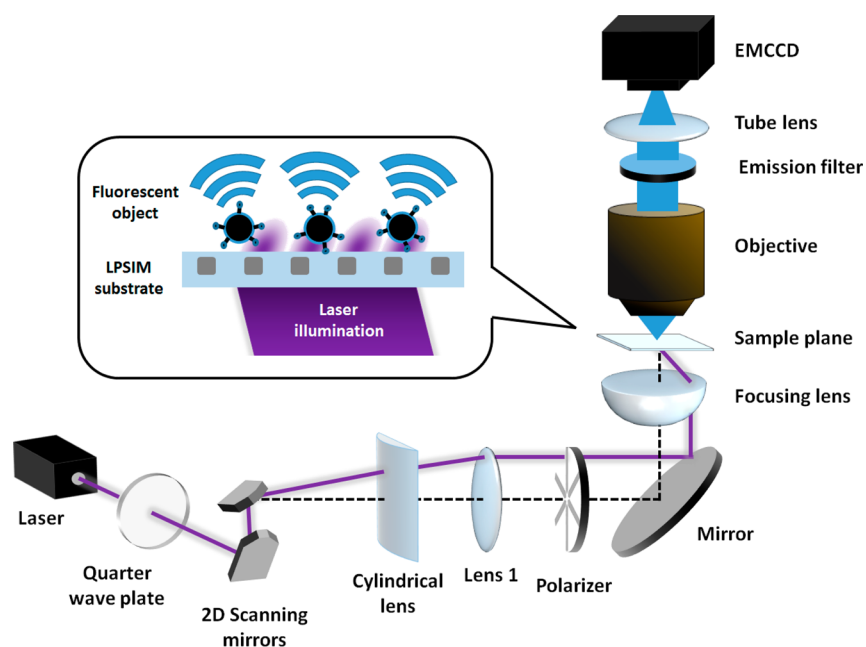


Figure 2. Schematics of the experimental imaging setup. An excitation laser is directed *via* 2D scanning mirrors through a high-NA 4f system that dictates the angle and plane of laser incidence to the nanoantenna array. In-plane polarization regardless of angle is guaranteed by a custom-made polarizer plate, which ensures the correct excitation patterns are formed. Emitted fluorescence is collected by the objective, filtered, and passed to the EMCCD. Inset: At the sample plane, fluorescent-tagged objects are selectively excited by LP fields with fine-grained spatial dependence dictated by the nanoantenna geometry and the incident laser angle.

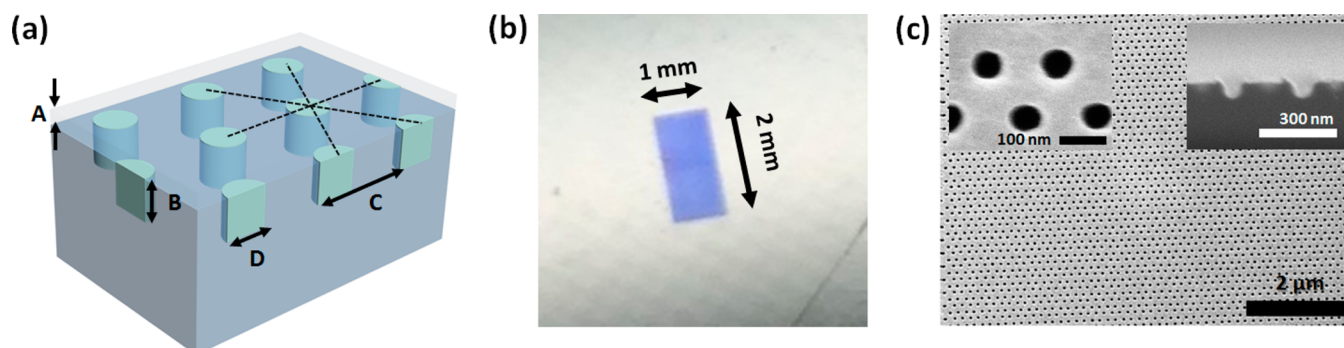


Figure 3. (a) 3D schematic of an LPSIM substrate composed of a silver nanodisc array embedded in glass.  $A = 20$  nm is the protective layer thickness.  $B = 60$  nm is the disc height.  $C = 150$  nm is the pitch.  $D = 60$  nm is the disc diameter. (b) Backlit photograph of full patterned area, showing uniform blue/violet LP response of silver discs. (c) SEM image of nanodisc array mold from above, showing the hexagonal lattice geometry. Scale bar:  $2 \mu\text{m}$ . Left inset: The same mold at a higher magnification. Scale bar:  $100$  nm. Right inset: Cross-sectional SEM image of an intermediate substrate just prior to silver deposition, showing cavities with  $60$  nm depth ready to be filled by silver. The scale bar represents  $300$  nm.

the key to the desired super-resolution performance. The height and diameter of the nanodiscs were tuned to optimize the variability and coverage of the full object plane from pattern to pattern, to satisfy the requirements of our reconstruction scheme. This design was verified by full wave simulations and analytical imaging calculations prior to fabrication.

To get the super-resolution image information, a total of nine diffraction-limited subimages were collected for each LPSIM image frame. Taking advantage of the 3-fold symmetry of our array, the angle was varied three times in each of three planes of incidence, always with in-plane polarization. The fluorescent samples were placed directly on the plasmonic substrate, so that the evanescently bound LP fields would have a strong effect. Once the subimages were collected, a straightforward reconstruction algorithm<sup>27</sup> allowed for an accurate recovery

of the super-resolution image, even when the plasmonic excitation patterns were not precisely known.

We devised a fabrication process using nanoimprinting to allow for repeated, reliable production of many LPSIM substrates without excessive time or cost, as shown in Figure S3 (see Supporting Information for details). A protective layer of  $\text{SiO}_2$  was sputtered on top of the silver antenna array. This layer serves multiple purposes, and the chosen thickness of  $20$  nm is carefully optimized. It protects the silver from oxidation and handling damage, it prevents fluorescence quenching, and it protects biological samples from direct contact with silver, with only minimal separation of the object from the evanescent LP field excitation. The protective layer also makes reuse of the substrate possible, provided that the fluorescent sample can be gently removed.

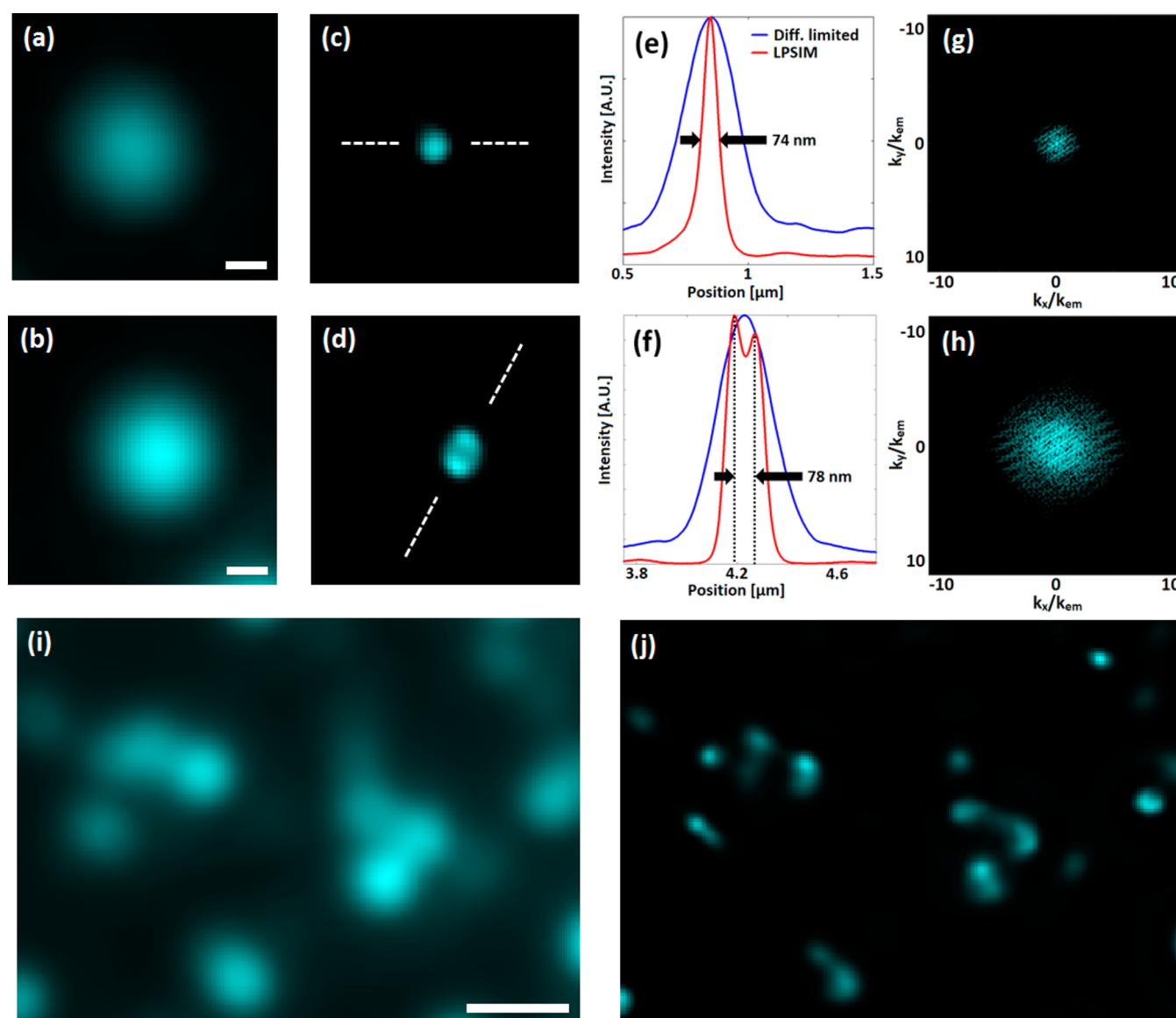


**Figure 4.** Demonstration of super-resolution performance. (a, b) Diffraction-limited images of a single and a pair of 50 nm fluorescent beads, respectively. Scale bars: 120 nm. (c, d) LPSIM image of (a) and (b) with significantly improved resolution, respectively. (e, f) Normalized intensity profiles of the images in (a, c) and (b, d), respectively, along the dashed white lines. (g, h) Spatial frequency spectra (log-scale amplitude) of a standard and an LPSIM image, respectively. The LPSIM technique increases the spatial bandwidth of the imaging process by a factor of approximately 3. (i, j) Diffraction-limited and LPSIM images of many beads within a wider area. Scale bar: 0.5  $\mu\text{m}$ .

Shown in Figure 3c are SEM images of the real LPSIM geometry from above, and from a cross-section view, at different stages of the fabrication process. Good uniformity is observed over a wide area, which is essential to final image quality. This uniformity is also shown at a larger scale by the camera image in Figure 3b.

### LPSIM SUBSTRATE FABRICATION

The fabrication of our LPSIM substrates was centered on a nanoimprinting process to ensure cost-effective, timely repeatability. All fabrication steps took place in the Nano3 cleanroom facility at University of California, San Diego. The master mold was formed on a silicon wafer. A 60 nm layer was oxidized and then spin coated with poly(methyl methacrylate) (PMMA). Electron beam lithography (EBL) patterning of the hexagonal array geometry was done with a Vistec EBPG5200. The pattern was etched into the oxidized layer. All etching steps

in this fabrication process were done with an Oxford Plasmalab 80. After lift-off of the resist layer, the master mold was coated with a nonstick vapor treatment. The stamp polymer, shaped by the master mold, was adhered to a glass wafer in an ultraviolet oven to create the soft nanoimprint stamp. The LPSIM substrate began with a fused silica wafer, coated with a 300 nm PMMA resist underlayer, and then a 70 nm top layer of UV resist (I-UVP, EZ Imprinting). This bilayer resist was stamped using an EVG620 mask alignment system. The nanoimprinted pattern was etched into the fused silica LPSIM substrate. Metal deposition was done with a Temescal BJD 1800 electron beam evaporator and included a 2 nm titanium adhesion layer. After lift-off of the resist and unwanted metal, a 20 nm spacer layer of  $\text{SiO}_2$  was deposited with a Denton Discovery 18 sputtering system.

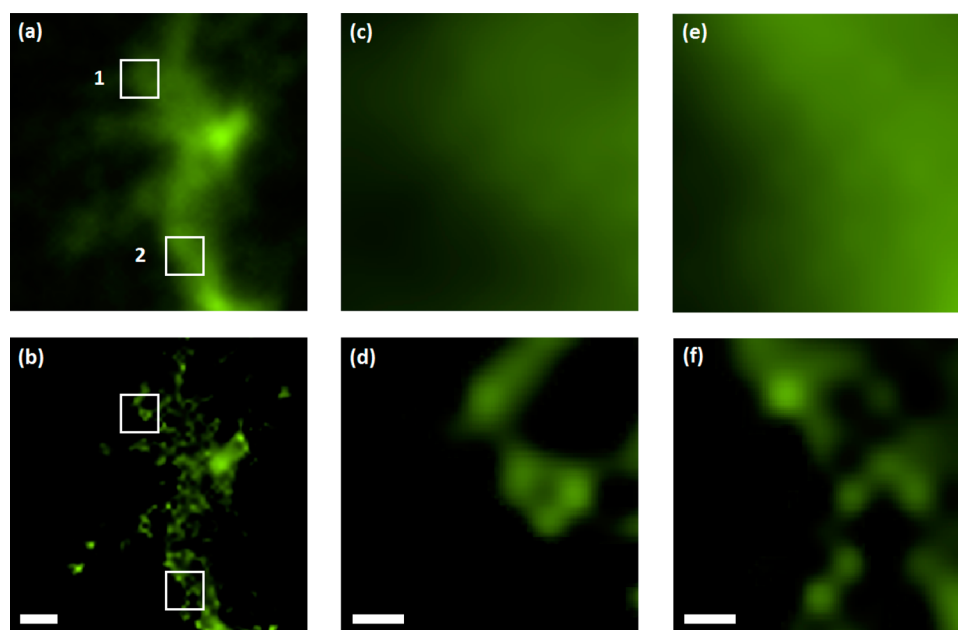


**Figure 5.** LPSIM fluorescence imaging results for a fixed neuron cell, showing Fzd3 receptors labeled with tdTomato. A 150 mW, 488 nm laser was used for illumination. The central fluorescence wavelength was 570 nm. (a, b) Wide-field diffraction-limited and LPSIM images, showing consistent, dramatic resolution enhancement over the full area. Scale bar: 500 nm. (c, d) Closer look at the area inside box 1 from (a) and (b), showing clear resolution improvement, consistent with theoretical expectations. Scale bar: 100 nm. (e, f) Closer look at the area inside box 2. Scale bar: 100 nm.

## RESULTS AND DISCUSSION

Characterization of the resolving power was done by looking at both single-bead full-width at half-maximum (fwhm) as well as two-bead separation. Figure 4a,c,e show the imaging results of a single bead, with an LPSIM fwhm of just 74 nm, which is approximately one-third the diffraction-limited fwhm, as expected. Figure 4b,d,f show two closely spaced beads, which are unresolvable under normal imaging conditions, but can be clearly resolved *via* LPSIM. The center-to-center spacing of the beads was 78 nm, which means the edge-to-edge gap between them was approximately 28 nm. Figure 4g,h show the Fourier space results for the real-space distribution of beads shown in Figure 4i,j, both with and without the LPSIM technique applied. We find that the effective OTF radius is tripled by the LPSIM technique, in agreement with the expected 3 $\times$  improvement. Over a wide area, a clean, super-resolved image is obtained, with minimal distortion.

One motivation for super-resolution imaging is to be found in cellular biology. Genomic and neuronal activities in particular are hot areas of research. As an initial demonstration of biocompatibility and general imaging capability, we used our LPSIM technique to image neuron cells expressing Fzd3-tdTomato. This particular type of sample is of interest<sup>28</sup> in understanding how growth cones steer themselves within their environment. Relevant features of Fzd3-containing vesicles can be as small as 50 to 100 nm in diameter. LPSIM is well-suited for use with this type of sample. For the tdTomato emission, the minimum resolvable feature size under the diffraction limit was 240 nm, but using LPSIM we observe resolution down to  $\sim$ 80 nm. As shown in Figure 5, important subcellular features can be imaged at much greater resolution ( $\sim$ 3 $\times$ ) compared with the diffraction-limited case. Due to the evanescent nature of localized plasmons, LPSIM is best applied to imaging objects that are either very thin or on the surface of a thicker object. In this sample, focal adhesions are directly on the surface of the

neuron cell, making them very convenient to image. In fact, this z-confinement of the excitation pattern can be advantageous if the goal is to only image a very thin slice of an object near the surface. Because the fluorescence wavelength in this experiment was longer, the resolution achieved was slightly less. However, silver is still a good plasmonic material at 488 nm laser wavelength, and the *k*-space collection scheme is still valid. The blind reconstruction algorithm, with the proper physical and statistical constraints, does a good job of de-emphasizing background noise and accounting for discrepancies between the theoretically expected excitation patterns and the actual experimental reality.

## CONCLUSIONS

In many practical cases, the LPSIM technique offers an optimal balance between the many factors influencing the usefulness of an image to biologists. LPSIM does not require point scanning to generate the image. The nanoantenna fields are scanned in parallel, so the field of view is limited only by optics and the area of the fabricated substrate itself and can be increased without sacrificing imaging speed. The resonant LP fields decay exponentially away from the substrate. Therefore, the vast majority of the fluorescent signal comes from the surface of the object, as is essential for fluorescent imaging. Additional postprocessing can be used<sup>29</sup> to remove any remaining out-of-plane noise. The resonant plasmonic enhancement of the LP fields in our optimized structure provides several advantages. For one, the local enhancement allows for strong excitation of the targeted fluorescent labels without using an unnecessarily high-powered laser or irradiating the entire sample with strong intensity. In our experiments, the intensity incident to the LPSIM substrate was just 5 W/cm<sup>2</sup>. The resonant excitation also holds potential for shorter exposure times and faster imaging speed, since the strongly excited signal will be boosted relative to the noise sources present in a given experiment.

The super-resolution performance achieved in this work was consistent and robust for various samples tested. The resolution of LPSIM could be incrementally improved to sub-50 nm scales by using shorter laser wavelengths or a higher-NA objective, in combination with an appropriately designed LPSIM substrate. Due to the dependence of LP resonances on particle size,<sup>30</sup> and the various emission spectra of available fluorescent dyes, this technique is readily scalable to different operating wavelengths. To push resolution even further, more complex substrate designs possibly incorporating both LP and SPP structure into the excitation patterns may hold promise. The technique shown here should prove useful for a multitude of fluorescence imaging applications, especially for biological surface dynamics.

## METHODS/EXPERIMENTAL

The illumination lasers used for the images shown in this work were a Coherent OBIS 405 LX and a Coherent Sapphire 488. The linearly polarized output laser light was passed through a quarter-wave plate, providing circular polarization incident to a custom polarizer plate that passively picks out the desired in-plane polarization to pass to the nanoantenna array. The laser beam profile was cleaned using a pinhole placed in the Fourier plane between two lenses. The 2D scanning mirror system used was a Cambridge Technology MicroMax 673. A Zeiss Axioskop 2 microscope with motorized objective control was used for fluorescence imaging. Images were recorded with an Andor iXon 897 EMCCD, with 0.1–0.6 s exposure time. A dichroic beamsplitter and a band-stop emission filter were used to separate the fluorescent signal. A custom sample stage, translatable in three dimensions, was used to position the sample relative to the 4f system.

To test the super-resolution performance of our LPSIM setup, a random distribution of fluorescent polystyrene beads was used as a test object. The beads were 50 nm in diameter and were excited by a 405 nm laser with an initial output power of 150 mW. The beads (Fluoresbrite YG microspheres) exhibited filtered fluorescent emission centered around 500 nm. Beads were drop-cast directly onto the LPSIM substrate, fixed, and imaged with an Olympus UPLSAPO 60× water immersion objective (NA = 1.2). Another neuron cell sample was prepared to demonstrate the biocompatibility of the LPSIM method. Rat E13 embryos of either sex were eviscerated, and the notochord was removed. Using a pulled glass needle, Fzd3-tdTomato-expressing plasmids<sup>28</sup> were injected into the neural tube. Using 5 mm gold-plated electrodes (#45-0115; Harvard Apparatus, South Natick, MA, USA), square-wave current was passed across the dorsal neural tube using a BTX #ECM 830 electroporator. Electroporation conditions were as follows: three pulses, 25 V, 100 ms pulse, 1 s interval. After electroporation, the spinal cord was dissected and dissociated commissural neurons were plated on the matrix coated with 20 μg/mL poly-D-lysine. After 2 days *in vitro*, the neurons were fixed in 4% paraformaldehyde for 15 min at 37 °C and mounted in Fluoromount G. Experiments were conducted in accordance with the NIH Guide for the Care and Use of Laboratory Animals and approved by the UCSD Animal Subjects Committee.

## ASSOCIATED CONTENT

### Supporting Information

The Supporting Information is available free of charge on the ACS Publications website at DOI: 10.1021/acsnano.7b01158.

Information about super-resolution image reconstruction, details about the LPSIM fabrication procedure, and details about the experimental imaging setup (PDF)

## AUTHOR INFORMATION

### Corresponding Author

\*E-mail: zhaowei@ucsd.edu.

## ORCID

Joseph L. Ponsetto: 0000-0003-0364-6782

Anna Bezryadina: 0000-0002-9776-5477

Hao Shen: 0000-0002-0063-3153

## Notes

The authors declare no competing financial interest.

## ACKNOWLEDGMENTS

The authors acknowledge financial support from the Gordon and Betty Moore Foundation.

## REFERENCES

- (1) Axelrod, D. Total Internal Reflection Fluorescence Microscopy in Cell Biology. *Traffic* **2003**, *2*, 764–774.
- (2) Mizusawa, K.; Takaoka, Y.; Hamachi, I. Specific Cell Surface Protein Imaging by Extended Self-Assembling Fluorescent Turn-On Nanoprobes. *J. Am. Chem. Soc.* **2012**, *134*, 13386–13395.
- (3) Canović, E. P.; Seidl, D. T.; Polio, S. R.; Oberai, A. A.; Barbone, P. E.; Stamenović, D. Biomechanical Imaging of Cell Stiffness and Prestress with Subcellular Resolution. *Biomech. Model. Mechanobiol.* **2014**, *13*, 665–678.
- (4) Schmoranzler, J.; Goulian, M.; Axelrod, D.; Simon, S. M. Imaging Constitutive Exocytosis with Total Internal Reflection Microscopy. *J. Cell Biol.* **2000**, *149*, 23–32.
- (5) Lakämper, S.; Kallipolitou, A.; Woehlke, G.; Schliwa, M.; Meyhöfer, E. Single Fungal Kinesin Motor Molecules Move Processively along Microtubules. *Biophys. J.* **2003**, *84*, 1833–1843.
- (6) Gustafsson, M. G. L. Surpassing the Lateral Resolution Limit by a Factor of Two Using Structured Illumination Microscopy. *J. Microsc.* **2000**, *198*, 82–87.
- (7) Keller, P. J.; Schmidt, A. D.; Santella, A.; Khairy, K.; Bao, Z.; Wittbrodt, J.; Stelzer, E. H. K. Fast, High-Contrast Imaging of Animal Development with Scanned Light Sheet-Based Structured Illumination Microscopy. *Nat. Methods* **2010**, *7*, 637–643.
- (8) Rust, M. J.; Bates, M.; Zhuang, X. Sub-Diffraction-Limit Imaging by Stochastic Optical Reconstruction Microscopy (STORM). *Nat. Methods* **2006**, *3*, 793–796.
- (9) Lu, D.; Liu, Z. Hyperlenses and Metalenses for Far-Field Super-Resolution Imaging. *Nat. Commun.* **2012**, *3*, 1205.
- (10) Wan, W.; Ponsetto, J. L.; Liu, Z. Numerical Study of Hyperlenses for Three-Dimensional Imaging and Lithography. *Opt. Express* **2015**, *23*, 18501–18510.
- (11) Willig, K. I.; Harke, B.; Medda, R.; Hell, S. W. STED Microscopy with Continuous Wave Beams. *Nat. Methods* **2007**, *4*, 915–918.
- (12) Betzig, E.; Patterson, G. H.; Sougrat, R.; Lindwasser, O. W.; Olenych, S.; Bonifacino, J. S.; Davidson, M. W.; Lippincott-Schwartz, J.; Hess, H. F. Imaging Intracellular Fluorescent Proteins at Nanometer Resolution. *Science* **2006**, *313*, 1642–1645.
- (13) Liu, Z.; Durant, S.; Lee, H.; Pikus, Y.; Fang, N.; Xiong, Y.; Sun, C.; Zhang, X. Far-Field Optical Superlens. *Nano Lett.* **2007**, *7*, 403–408.
- (14) Gustafsson, M. G. L. Nonlinear Structured Microscopy: Wide-Field Fluorescence Imaging with Theoretically Unlimited Resolution. *Proc. Natl. Acad. Sci. U. S. A.* **2005**, *102*, 13081–13086.
- (15) Saxena, M.; Gangadhar, E.; Gorthi, S. S. Structured Illumination Microscopy. *Adv. Opt. Photonics* **2015**, *7*, 241–275.
- (16) Kner, P.; Chhun, B. B.; Griffis, E. R.; Winoto, L.; Gustafsson, M. G. L. Super-Resolution Video Microscopy of Live Cells by Structured Illumination. *Nat. Methods* **2009**, *6*, 339–342.
- (17) Schermelleh, L.; Carlton, P. M.; Haase, S.; Shao, L.; Winoto, L.; Kner, P.; Burke, B.; Cardoso, M. C.; Agard, D. A.; Gustafsson, M. G. L.; Leonhardt, H.; Sedat, J. W. Subdiffraction Multicolor Imaging of the Nuclear Periphery with 3D Structured Illumination Microscopy. *Science* **2008**, *320*, 1332–1336.
- (18) Li, D.; Shao, L.; Chen, B.; Zhang, X.; Zhang, M.; Moses, B.; Milkie, D. E.; Beach, J. R.; Hammer, J. A.; Pasham, M.; Kirchhausen,

T.; Baird, M. A.; Davidson, M. W.; Xu, P.; Betzig, E. Extended-Resolution Structured Illumination Imaging of Endocytic and Cytoskeletal Dynamics. *Science* **2015**, *349*, 349, aab3500.10.1126/science.aab3500

(19) Wei, F.; Liu, Z. Plasmonic Structured Illumination Microscopy. *Nano Lett.* **2010**, *10*, 2531–2536.

(20) Wei, F.; Lu, D.; Shen, H.; Wan, W.; Ponsetto, J. L.; Huang, E.; Liu, Z. Wide-Field Super-Resolution Surface Imaging through Plasmonic Structured Illumination Microscopy. *Nano Lett.* **2014**, *14*, 4634–4639.

(21) Barnes, W. L.; Dereux, A.; Ebbesen, T. W. Surface Plasmon Subwavelength Optics. *Nature* **2003**, *424*, 824–830.

(22) Fernandez-Dominguez, A. I.; Liu, Z.; Pendry, J. B. Coherent Four-Fold Super-Resolution Imaging with Composite Photonic-Plasmonic Structured Illumination. *ACS Photonics* **2015**, *2*, 341–348.

(23) Ponsetto, J. L.; Wei, F.; Liu, Z. Localized Plasmon Assisted Structured Illumination Microscopy for Wide-Field High-Speed Dispersion-Independent Super Resolution Imaging. *Nanoscale* **2014**, *6*, 5807–5812.

(24) Willets, K. A.; Van Duyne, R. P. Localized Surface Plasmon Resonance Spectroscopy and Sensing. *Annu. Rev. Phys. Chem.* **2007**, *58*, 267–297.

(25) Oster, G.; Wasserman, M.; Zwerling, C. Theoretical Interpretation of Moiré Patterns. *J. Opt. Soc. Am.* **1964**, *54*, 169–175.

(26) Gustafsson, M. G. L.; Agard, D. A.; Sedat, J. W. Doubling the Lateral Resolution of Wide-Field Fluorescence Microscopy using Structured Illumination. *Proc. SPIE* **2000**, *3919*, 141–150.

(27) Mudry, E.; Belkebir, K.; Girard, J.; Savatier, J.; Le Moal, E.; Nicoletti, C.; Allain, M.; Sentenac, A. Structured Illumination Microscopy using Unknown Speckle Patterns. *Nat. Photonics* **2012**, *6*, 312–315.

(28) Onishi, K.; Shafer, B.; Lo, C.; Tissir, F.; Goffinet, A. M.; Zou, Y. Antagonistic Functions of Dishevelleds Regulate Frizzled3 Endocytosis via Filopodia Tips in Wnt-Mediated Growth Cone Guidance. *J. Neurosci.* **2013**, *33*, 19071–19085.

(29) Neil, M. A. A.; Juškaitis, R.; Wilson, T. Method of Obtaining Optical Sectioning by using Structured Light in a Conventional Microscope. *Opt. Lett.* **1997**, *22*, 1905–1907.

(30) Kelly, K. L.; Coronado, E.; Zhao, L. L.; Schatz, G. C. The Optical Properties of Metal Nanoparticles: The Influence of Size, Shape, and Dielectric Environment. *J. Phys. Chem. B* **2003**, *107*, 668–677.